University of Groningen

Anisotropies In The Cosmic Microwave Background: A Two Fluid Approximation

Bachelor's Thesis

To fulfill the requirements for the degree of
Bachelor of Physics
at University of Groningen under the supervision of
Prof. dr. D. Roest (Van Swinderen Institute, University of Groningen),
Prof. dr. D. Meerburg (Van Swinderen Institute, University of Groningen)
and
T.W.J. de Wild (Physics Lecturer, University of Groningen)

Alfonso Puicercus Gomez (s3938107)

July 8, 2022

Contents

Acknowledgments

I would like to thank Prof. dr. Daan Meerburg for providing the topic of research of this thesis and enlightenment with helpful insights. I would also like to thank T.W.J de Wild for the continuous support and problem resolution which have made this project far more enjoyable.

Abstract

This thesis introduces a conceptually simple method for the calculation of the anisotropy power spectrum of the cosmic microwave background using a two-fluid approximation. Evaluating the set of coupled fluid equations at recombination for both small and large scales regimes and free-streaming the solutions until today gives the CMB anisotropies. The model successfully reproduces the physical processes involved in the creation of these fluctuations to great accuracy, therefore making it a suitable approach for a better understanding of the physics behind the temperature anisotropies. Moreover, the toy model being considered is sensitive to a high degree to most of the critical parameters usually considered in different cosmological models, which can be used to comprehend the behaviour of the peaks. The code was developed in Python and is simple enough to be modified easily, both for the variation of the cosmological parameters and the possible implementation of more precise effects or approximations.

1 Introduction

The Cosmic Microwave Background (CMB) is certainly one of the strongest pieces of evidence and data to analyze. It can be used to comprehend multiple aspects of our Universe such as the matter/radiation content or a test for cosmological models. Thanks to improved satellite experiments, anisotropies can be observed on the temperature map of the CMB.

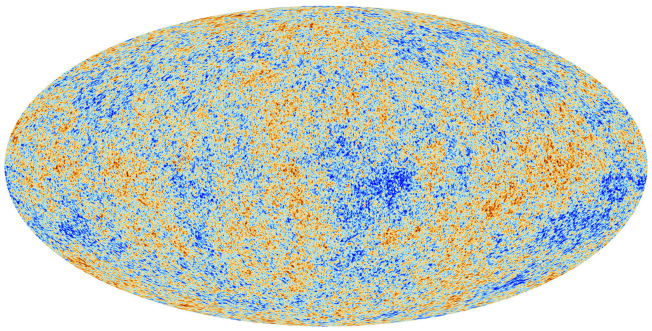

Figure 1: Cosmic Microwave Background temperature map (image created from the Planck spacecraft data [5])

For a full understanding of how these temperature anisotropies were created and how they have evolved due to the accelerating expansion of the Universe, many aspects have to be taken into account, such as inflation in the early Universe to resolve Big Bang cosmology complications, cosmological perturbation theory and structure formation in later epochs.

Inflation is a mechanism that produces the exponential expansion of space and explains the observed homogeneous and isotropic Universe [3]. Due to the nature of the inflaton field associated with the inflation mechanism quantum fluctuations occurred, which then translated into fluctuations in the spacetime metric. The early Universe fluid containing all matter and energy, influenced by these perturbations, produced density inhomogeneities which then caused the observable temperature anisotropies in the CMB.

The description of the development and progression of the CMB anisotropies is obtained from solving the coupled equations of the different particle species, these being the Euler, Continuity and Boltzmann equations. A full CMB analysis is complex since this set of coupled differential equations is somewhat intricate. This is the reason why the approach presented uses a simplified toy-model describing how the CMB temperature anisotropies depend on cosmological parameters.

In this thesis, the derived approach makes use of a two fluid approximation using gauge invariant perturbation theory to reproduce the CMB power spectrum. The toy-model will be examined in order to see how well it resembles the full calculation of the temperature anisotropies when cosmological parameters are varied. As it will be shown, even though the use of a two fluid approximation is made, the formation of the temperature anisotropies is complicated. The physical background needed for the understanding of these fluctuations will be provided.

The toy-model is able to create a power spectrum which matches to great accuracy the obtained by more complex models, therefore making it useful for the understanding of this topic in cosmology.

2 Background Literature

There is plenty of observational evidence that the Universe is driven by an accelerating expansion since the Big Bang. Thanks to the investigation of this expansion, the history of the Universe, also known as the Thermal History, can be studied and divided into different epochs depending on the significant events happening such as the temperature/energy or decoupling of the multiple particle species from the plasma. Some of these concepts will be explored in this section as an introduction for a better comprehension of this thesis.

2.1 The CMB Temperature Map

Based on the Big Bang theory, the cosmological principle should be held, meaning that on large scales the Universe should be homogeneous and isotropic. As mentioned in the introduction, the CMB temperature map presents an almost perfectly isotropic and homogeneous distribution, with an average temperature of $T = 2.7548 \pm 0.00057K$ [4]. However, as it can be observed from Figure 1, the temperature map exhibits inhomogeneities.

If the Universe were to be homogeneous and isotropic, the CMB temperature map would also have the same properties, thus, the temperature map would have the same average temperature over all space. In other words, Figure 1 would have the same color at every single point. The fact that the temperature map still presents such uniformity sustains the theory of the Big Bang and the ΛCMD model, which is a parameterized Big Bang model which will be explained in the following subsection.

The fact that the observed temperature map is in accordance with the cosmological principle means that the early Universe would have been in thermal equilibrium. However, for a system to be in thermal equilibrium, the particles must have enough time for anisotropies to vanish. This presents a problem. Since the expansion of the Universe is so rapid, the contents of it would not have had enough time to reach thermal equilibrium due to the patches of space moving faster than the speed of light, thus, the regions would have never been in causal contact. This problem is fixed with inflation, which sets the well known homogenous and isotropic Universe and introduces quantum fluctuations which cause spacetime metric perturbations that become the temperature anisotropies observed in the CMB.

A point has to be made here, inflation is a mechanism that solves multiple problems such as the one introduced above, however, it has not been experimentally proven but it is one of the few theories of the early Universe that produces these characteristics. As will be shown later in this thesis, fluctuations on scales larger than the horizon at recombination are coherent [3]. This coherence is either achieved by inflation, other mechanisms or requires unnatural fine-tunning to have this feature.

2.2 Our Universe

2.2.1 Main Components

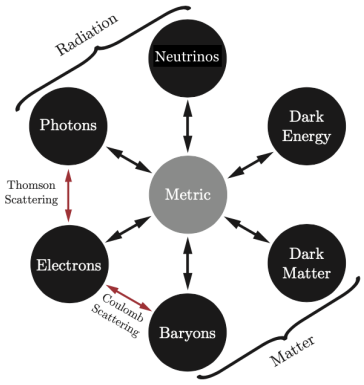

Figure 2: Interactions between the cosmological components (figure adapted from [1])

The parameterization of the Big Bang model can be done in multiple ways, however, one of the most famous models is the aforementioned ΛCMD model. This particular cosmological model implements radiation, although its value is usually low compared to the other cosmological parameters at today conformal time.In the past it was the dominant source of density. This model can be expanded with dark energy associated with the cosmological constant Λ, cold dark matter (CDM) which is a type of dark matter that moves slow compared to the speed of light, and ordinary matter. This model successes to explain various properties of the Universe while being relatively simple, is perhaps the reason of its popularity. In Figure 2, the parametrization of the cosmological quantities is expanded into the commonly known particle species.

In the very early stages of the Universe, a unique fluid containing all the radiation, matter, CDM and dark energy governed the physics. However, as shown in Figure 2, each particle species interacts differently with the other contributors of the fluid, some of them coupling to each other, some only affecting the rest indirectly. It will be studied in detail that all the different cosmological quantities modify the spacetime metric and viceversa.

This is fact is key since it can be used to relate the metric perturbations due to inflation to the density fluctuations that later cause the temperature anisotropies. Nevertheless, the set of differential coupled equations that model the physics behind the species in the fluid is complicated and a two fluid approximation will be introduced.

2.2.2 Thermal History

From the hot dense fluid containing all in the early Universe, the different particle species started to decouple while spacetime expanded. Due to the expansion of the Universe, the overall temperature, and therefore the energy of the plasma, reduced eventually allowing the decoupling of photons to happen.

Event	time t	redshift z	temperature T
Singularity	**0**	**∞**	**∞**
Quantum gravity	$\sim 10^{-43}$ s	–	$\sim 10^{18}$ GeV
Inflation	$\gtrsim 10^{-34}$ s	–	–
Baryogenesis	$\lesssim 20$ ps	$> 10^{15}$	> 100 GeV
EW phase transition	20 ps	10^{15}	100 GeV
QCD phase transition	20 μs	10^{12}	150 MeV
Dark matter freeze-out	?	?	?
Neutrino decoupling	1 s	6×10^9	1 MeV
Electron-positron annihilation	6 s	2×10^9	500 keV
Big Bang nucleosynthesis	3 min	4×10^8	100 keV
Matter-radiation equality	60 kyr	3400	0.75 eV
Recombination	260–380 kyr	1100–1400	0.26–0.33 eV
Photon decoupling	380 kyr	1100	0.26 eV
Reionization	100–400 Myr	10–30	2.6–7.0 meV
Dark energy-matter equality	9 Gyr	0.4	0.33 meV
Present	**13.8 Gyr**	**0**	**0.24 meV**

Figure 3: Thermal history of the Universe (figure adapted from [2])

As shown in Figure 3, the Universe underwent a series of eras, each marking a key point in the evolution. For the purpose of this thesis, not all of the above eras have to be studied in detail. Therefore, only the most important epochs influencing the physics described by the equations later derived will be explained. Since the CMB is the temperature map from the photons that last decoupled, there will be two key eras describing where those photons come from.

The first period of interest is *recombination* which is the time at which neutral hydrogen is formed through the reaction of an electron and a proton giving a hydrogen atom and energy released associated with a photon $e^- + p^+ \rightarrow \mathrm{H} + \gamma$. Neutral hydrogen could have already formed in the Big Bang nucleosynthesis era but the temperature is still not low enough and the reverse process could still occur. However, during recombination, the temperature is low enough that the reverse reaction cannot happen. This would cause the free electron density to decrease greatly and the mean free path of the photons increased longer than the horizon. These are the photons observed in the CMB.

Photon decoupling follows the recombination era. These two eras are strongly related since they both occur when the Universe is 380.000 years old. Although photon decoupling happens in recombination, the reaction in this era only involved the decoupling of photons from electrons $e^- + \gamma \leftrightarrow e^- + \gamma$. As aforementioned, the electron density drops during recombination and therefore, the interaction rate between electrons and photons decreases. When the interaction rate is approximately equal to the horizon scale, the photons and electrons decoupled.

3 Evolution of Cosmological Perturbations

As mentioned in the Introduction, modeling the evolution of cosmological perturbation can be acquired by solving the coupled equations, those being the Boltzmann, Euler and continuity equations depending on the particle species. The state of the universe and its content varies while expands and freezes out, forcing species to decouple from the hot dense plasma.

Considering homogeneous fluids which account for all the content of the early Universe and introducing first order perturbations is sufficient to describe the temperature fluctuations observed in the CMB. The evolution of these anisotropies can be studied using cosmological perturbation theory. However, finding all the evolution equations can be complex and, as it will be shown, not required since only considering a photon-baryon fluid and a cold dark matter (CDM) fluid is an acceptable approximation.

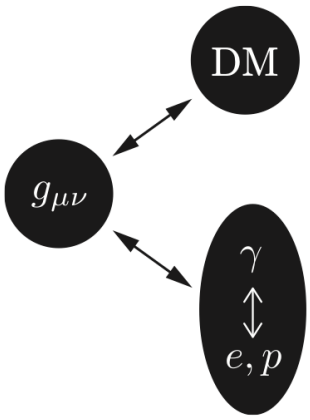

Figure 4: Two fluid approximation illustration (figure adapted from [3])

The photon-baryon fluid is *one* fluid before recombination thanks to the so called *tight coupling* limit, which assumes rapid Thomson scattering between photons and baryons. The tight coupling limit breaks down after recombination when photons decouple from the plasma, which will be further explained. It is common in this area of cosmology to refer to baryons as protons and electrons even though electrons are not part of that family of particles. Protons and electrons are coupled/interact via Coulomb interaction but it is so rapid that they can be considered to be together as a unique entity/species.

The need for the tight coupling limit comes from the fact that considering a hydrodynamic approach for the early universe plasma, that being treating it as a fluid, reduces the complexity of the equations, making them only dependent on the density, flow velocity and shear. When considering a kinetic approach, this corresponds to monopole, dipole and quadrupole moments respectively. As it will be presented later on, higher multipole moments are not considered as they are suppressed.

As previously mentioned, the CDM is not being considered in the same photon-baryon fluid and it will be considered in a separate fluid thus leading to a *two fluid approximation*.

3.1 Coupled Fluid Equations

The two fluids being considered couple to each other only gravitationally and therefore, their energy-momentum tensors are conserved separately, from which it is possible to obtain their equations of motion. Since the focus of this thesis is to study the temperature anisotropies observed in the CMB, only scalar perturbations are taken into account. These scalar perturbations can be defined in the density as,

$$\rho = \bar{\rho} + \delta\bar{\rho} = \bar{\rho}(1+\delta) \quad \text{where} \quad \delta = \frac{\delta\rho}{\bar{\rho}} \tag{1}$$

The evolution of the scalar perturbations of an uncoupled fluid is described by the continuity equation for density fluctuations δ and the Euler equation for the divergence of the velocity field θ of the fluid,

$$\begin{aligned}\delta' &= -(1+w)\left(\theta - 3\Phi'\right) - 3\mathcal{H}\left(c_s^2 - w\right)\delta\,,\\ \theta' &= -\mathcal{H}(1-3w)\theta - \frac{w'}{1+w}\theta + \frac{c_s^2}{1+w}k^2\delta + k^2\Phi \;\text{ where }\; \theta = \vec{\nabla}\cdot\vec{v}\,.\end{aligned} \tag{2}$$

These equations are dependent on the equation of state $w = p/\rho$, sound speed $c_s^2 = \delta p/\delta\rho$, Fourier wavemode k, Hubble parameter $\mathcal{H} = a'/a$, and Φ which is essentially the metric perturbation although it will be sometimes referred to as gravitational potential. These relationships change depending on the fluid being considered as their properties differ.

For CDM, the fluid equations (denoted with c as a subscript) are constrained by its pressureless nature, implying $w = c_s^2 = 0$ and therefore,

$$\delta_c' = -kv_c + 3\Phi', \quad v_c' = -\mathcal{H}v_c + k\Phi \tag{3}$$

For the photon-baryon fluid, w and c_s^2 are non-zero since photons exert a pressure $p_\gamma = \frac{1}{3}\rho_\gamma$. By defining a ratio R between the unperturbed overall baryon and photon density (the unperturbed quantity is denoted with an overhat), one can express the equation of state and sound speed in the following way,

$$w = \frac{1}{3+4R}, \quad c_s^2 = \frac{1}{3(1+R)}\,, \tag{4}$$

where

$$R = \frac{3}{4}\frac{\bar{\rho}_b}{\bar{\rho}_\gamma}\,. \tag{5}$$

In order to derive the coupled equations for the photon-baryon fluid, the tight coupling approximation has to be used. This suppresses the multipole moments higher than $l \geq 2$, when translated from the kinetic approach to the hydrodynamic view, only density and flow velocity needs to be considered [1]. This approximation implies,

$$\delta_b = \frac{3}{4}\delta_\gamma, \quad v_e = v_b = v_\gamma = -\Theta_1 \tag{6}$$

The equations describing the evolution of the photon-baryon fluid (denoted by γ as a subscript) are,

$$\delta_\gamma' = -\frac{4}{3}kv_\gamma + 4\Phi', \quad v_\gamma' = -\frac{R}{1+R}v_\gamma + \frac{1}{4(1+R)}k\delta_\gamma + k\Phi \tag{7}$$

Every coupled equation describing the evolution of both the CDM and the photon-baryon fluid has to be supplied with a set of equations directly derived from General Relativity, which are the linearized Einstein equation for the potential Φ and the Friedmann equation[1] for the background given below,

$$k\left(\Phi' + \mathcal{H}\Phi\right) = 4\pi G a^2 \sum_i \left(\bar{\rho}_i + \bar{p}_i\right) v_i \tag{8}$$

$$\mathcal{H}^2 = \left(\frac{a'}{a}\right)^2 = \frac{8\pi G a^2}{3}\sum_i \bar{\rho}_i \tag{9}$$

These equations directly involves General Relativity, which determines the evolution of space-time parameters to solve the coupled equations of both fluids. The analytical solution of Eq. (9) gives two important parameters, a, which is the expansion factor and τ being conformal time defined as,

$$y \equiv \frac{a}{a_{\rm eq}} = (\alpha x)^2 + 2\alpha x, \quad x \equiv \frac{\tau}{\tau_r}, \quad \alpha^2 \equiv \frac{a_{\rm rec}}{a_{\rm eq}}\,. \tag{10}$$

Here the equation is rescaled in conformal time over the conformal time τ_r given by,

$$\tau_r \equiv \left(\frac{4a_{\rm rec}}{\Omega_m H_0^2}\right)^{1/2}\,. \tag{11}$$

and the scale factor at recombination a_{rec} is rescaled over a_{eq} both taking the following values $a_{\rm rec}^{-1} \approx 1100, a_{\rm eq}^{-1} \approx 2.4 \times 10^4 \Omega_m h^2$.

[1] Both of the sums involved in the equations above are over both fluids.

Rescaled time x was introduced for numerical convenience and for the same reason, momentum is treated as $\kappa \equiv k\tau_r$ and the Hubble parameter is scaled as shown below,

$$\eta = \tau_r \mathcal{H} \equiv \frac{a'}{a} = \frac{1}{a}\frac{da}{dx} = \frac{2\alpha(\alpha x + 1)}{(\alpha x)^2 + 2\alpha x} \tag{12}$$

where the derivative in the scale factor is, as shown, over the new rescaled conformal time. The above equation was obtained by calculating the derivative w.r.t. x of the the scale factor a from Eq. (10) and using the usual definition of $\mathcal{H}$. In a similar way these rescaled parameters influence the derivatives, and the coupled equations take the following form,

$$\begin{aligned}
\delta_c' &= -\kappa v_c + 3\Phi' \\
v_c' &= -\eta v_c + \kappa\Phi, \\
\delta_\gamma' &= -\frac{4}{3}\kappa v_\gamma + 4\Phi' \\
v_\gamma' &= \left(1 + \frac{3}{4}y_b\right)^{-1}\left(-\frac{3}{4}y_b\eta v_\gamma + \frac{1}{4}\kappa\delta_\gamma\right) + \kappa\Phi
\end{aligned} \tag{13}$$

$$\Phi' = -\eta\Phi + \frac{3\eta^2}{2\kappa}\frac{v_\gamma\left(\frac{4}{3} + y - y_c\right) + v_c y_c}{1+y}. \tag{14}$$

with $y_{b,c} \equiv y\frac{\Omega_{b,c}}{\Omega_m}$. This is now the complete set of equations that describes the behaviour of the two fluids up to recombination, where the tight coupling approximation breaks down. The next step is obtaining the CMB fluctuations from the inhomogeneities at recombination which can be computed using the above formalism.

3.2 The Power Spectrum

So far, only the description of these fluids has been asserted. It will now be explained how the temperature anisotropies are obtained from the inhomogeneities. It is important to understand that the anisotropies observed in the temperature map of the CMB have been free-streaming since the time of recombination τ_{rec} until today at τ_0. By defining the location of the observed temperature perturbation at $\boldsymbol{x_0} \equiv \vec{0}$ and implementing the directional dependence on the sky with $\hat{\boldsymbol{n}}$ gives the following expression,

$$\tilde{\Theta}(\hat{\mathbf{n}}) \equiv \frac{\delta T}{T}(\hat{\mathbf{n}}) = \Theta\left(\tau_0, \mathbf{x}_0, \hat{\mathbf{p}} = -\hat{\mathbf{n}}\right) \tag{15}$$

which can be Fourier transformed into,

$$\tilde{\Theta}(\hat{\mathbf{n}}) = \int \frac{\mathrm{d}^3\mathbf{k}}{(2\pi)^{3/2}} e^{i\mathbf{k}\cdot\mathbf{x}_0}\Theta\left(\tau_0, \mathbf{k}, \hat{\mathbf{n}}\right) \tag{16}$$

Note that here the Fourier components k have been introduced, representing the wavenumber which is essentially the spatial frequency of the components of the temperature field. It is convenient to preform a multipole expansion[2] using $\Theta(\tau,\mu) = \Sigma(-i)^l\Theta_l(\tau)P_l(\mu)$,

$$\tilde{\Theta}(\hat{\mathbf{n}}) = \int \frac{\mathrm{d}^3\mathbf{k}}{(2\pi)^{3/2}} e^{i\mathbf{k}\cdot\mathbf{x}_0}\sum_l (-i)^l\Theta_l\left(\tau_0, \mathbf{k}\right)P_l(\hat{\mathbf{k}}\cdot\hat{\mathbf{n}}) \tag{17}$$

where the $P_l(\hat{\mathbf{k}}\cdot\hat{\mathbf{n}})$ is the Legendre polynomial. This expression can be further expanded in terms of a transfer function,

$$\tilde{\Theta}(\hat{\mathbf{n}}) = \int \frac{\mathrm{d}^3\mathbf{k}}{(2\pi)^{3/2}} e^{i\mathbf{k}\cdot\mathbf{x}_0}\sum_l (-i)^l\Theta_l(k)\mathcal{R}(\mathbf{k})P_l(\hat{\mathbf{k}}\cdot\hat{\mathbf{n}}) \tag{18}$$

where $\Theta_l(k) \equiv \frac{\Theta_l(\tau_0,\mathbf{k})}{\mathcal{R}(\mathbf{k})}$ is the transfer function aforementioned, and $\mathcal{R}(\mathbf{k})$ is the primordial curvature perturbation. This expression relates the transfer function to the primordial fluctuations generated during inflation. For the introduction of the power spectrum itself, an extra step on this derivation is required as well as some physical understanding of what is really being computed.

[2]The explicit k dependence of this equation has been removed for simplicity. This might also be done in further derivations but it will be recovered when it is necessary for a complete understanding of the physics.

When looking at the temperature map of the CMB, one can correlate the temperature fluctuations from two different directions $\hat{\mathbf{n}}$ and $\hat{\mathbf{n}}'$. Assuming that inflation lead to an statistically isotropic initial conditions, the only dependence that the correlation can have is the orientation. Thus, the two-point correlation between the temperature inhomogeneities from two different directions is found by using Eq. (18) as shown below,

$$\left\langle \tilde{\Theta}(\hat{\mathbf{n}})\tilde{\Theta}\left(\hat{\mathbf{n}}'\right)\right\rangle = \int \frac{\mathrm{d}^3\mathbf{k}}{(2\pi)^{3/2}}\frac{\mathrm{d}^3\mathbf{k}'}{(2\pi)^{3/2}} e^{i\left(\mathbf{k}+\mathbf{k}'\right)\cdot\mathbf{x}_0}\sum_l\sum_{l'}(-i)^{l+l'}\Theta_l(k)\Theta_{l'}\left(k'\right)\times\left\langle\mathcal{R}(\mathbf{k})\mathcal{R}\left(\mathbf{k}'\right)\right\rangle P_l(\hat{\mathbf{k}}\cdot\hat{\mathbf{n}})P_l(\hat{\mathbf{k}}'\cdot\hat{\mathbf{n}}') \tag{19}$$

After some manipulation which will be introduced later on, the expression takes the following form,

$$\left\langle \tilde{\Theta}(\hat{\mathbf{n}})\tilde{\Theta}\left(\hat{\mathbf{n}}'\right)\right\rangle = \sum_l \frac{2l+1}{4\pi}\left[\frac{4\pi}{(2l+1)^2}\int \mathrm{d}\ln k\ \Theta_l^2(k)\Delta^2_{\mathcal{R}}(k)\right]P_l\left(\hat{\mathbf{n}}\cdot\hat{\mathbf{n}}'\right) = \sum_l \frac{2l+1}{4\pi}C_l P_l\left(\hat{\mathbf{n}}\cdot\hat{\mathbf{n}}'\right) \tag{20}$$

Here, the term C_l, called angular power spectrum, is defined as,

$$C_l = \frac{4\pi}{(2l+1)^2}\int \mathrm{d}\ln k\ \Theta_l^2(k)\Delta^2_{\mathcal{R}}(k) \tag{21}$$

where $\Theta_l^2(k)$ is the transfer function introduced previously on this section and $\Delta^2_{\mathcal{R}}(k)$ is known as the primordial power spectrum and it takes the following form,

$$\Delta^2_{\mathcal{R}}(k) = A_s\left(\frac{k}{k_{pivot}}\right)^{n_s-1}, \tag{22}$$

New key parameters are introduced in the above equation. The first one, A_s, is the normalization parameter which just shifts the CMB power spectrum on the y-axis, therefore fixing the amplitude of the initial conditions. The parameter n_s regulates the tilt of the power spectrum, if $n_s = 1$ the spectrum would have equal power on all scales. The last parameter that appears is k_{pivot} which is just a value of the k-spectrum over which the primordial power spectrum is normalized. The values for these parameters will be given later. Note that all the last equations derived after the coupled equations are dependent on k not on the rescaled variable κ.

It would seem straightforward to now compute C_l from Eq. (21) for all the desired values of l but an expression for the transfer function has not been explicitly given. In order to find the transfer function, it is necessary to make a short deviation and recover the Boltzmann equation.

3.3 The Transfer Function

The photon-baryon plasma is tightly coupled by Compton scattering before recombination,. Thus, the Boltzmann equation implementing Compton scattering will describe the evolution of the temperature perturbations. For scalar fluctuations[3], the Boltzmann equation in Fourier space becomes [[1]],

$$\dot{\Theta} + ik\gamma\Theta = \dot{\Phi} - ik\gamma\Psi - \Gamma\left[\Theta - \Theta_0 - i\gamma v_e\right] \tag{23}$$

The time derivatives are over conformal time, as before. Two perturbation terms appear here, Ψ which is the gauge-invariant metric perturbation, and Φ, which is the potential describing the density perturbations accounting for all particle species. Both of these potentials become equal to each other if anisotropic stress is neglected [12], thus $\Psi \approx \Phi$[4]. The expression $k\gamma$ is the dot product between the k_i mode in the Fourier expansion and γ_i is the direction cosines[5] of the photon momentum. Another relevant variable which has not been introduced yet is the differential cross section to Thomson scattering Γ, and it is important later on when the recombination epoch is reached, as the equation that describes this parameter differs from earlier epochs. The term $-i\gamma v_e$ accounts for the amplitude of the baryon velocity.

[3]For the simplistic approach that is being taken in this study, only scalar fluctuations are being considered.

[4]This is the reason why Φ was described in Eq. (2) as the metric perturbation, although Ψ is really the parameter describing that exact physical effect

[5]The direction cosines are the cosines of the angles between the vector being considered and the three positive coordinate axes, following $\gamma \equiv \vec{k}\cdot\vec{p}$

Some of these terms have already appeared in past equations. To refresh what those terms are, here below are the relationships between the first multipole moments and δ_γ and v_γ,

$$\Theta_0 = \frac{1}{4}\delta_\gamma, \quad \Theta_1 = -v_\gamma \tag{24}$$

Getting back to the coupled equations (13), it is easy to see how these multipoles in the Boltzmann equations are related to the density perturbations. Many physical insights can be extracted, such as the gravitational potentials, referring to Φ and Ψ, which produce adiabatic growth and gravitational redshift on the temperature fluctuations. The most important aspect to note down from these formulas, is that the Newtonian potential Φ contributes directly to the velocity, as it can be seen in the Euler equation for both fluids, therefore causing an adiabatic growth of the perturbations. The physical interpretation is that inside the gravitational potential the fluid is compressed, but the pressure exerted by the photons restraints the increase in the density perturbations, thus forcing the gravitational potential to decay.

The gravitational redshift introduced on the temperature fluctuations is due to the gradient of the potential Ψ. This topic is explored in detail in [10]. The temperature perturbation after the photons have escaped the potential well Ψ at recombination is described by $\Theta+\Psi$ or by $\Theta+\Phi$ since Θ_0 describes the intrinsic temperature fluctuation and Ψ the change due to the photons climbing out of the potential well, which will be explained later on. The term Θ could already be used to describe the fluctuations, but not taking into account Ψ does not reflect the full effective perturbation. The gravitational potentials can evolve in time. The effect of this time dependence during the evolution of the universe until today is known as the integrated Sachs-Wolfe (ISW) effect and it referred to further in the thesis. The explanation of the physical insights involved in these equations is critical for the correct understanding of the following derivation.

In order to compute the observed CMB power spectrum, it is necessary to evolve the anisotropies at the surface of last-scattering forward in time until now, a process known as free-streaming. This can be done by integrating the Boltzmann equation along the line-of-sight. The line-of-sight can be referred to as the surface at a certain point in time from which light is received by the observer. In the case of the CMB, this is the surface from which photons last scattered from the plasma during recombination. The following derivation will show how to derive the free-streaming solution along the line of sight.

3.3.1 Last-scattering and Free-Streaming

For a better understanding of the formulas, two new concepts will be introduced, these being relevant both in the derivation below and for a future understanding of the power spectrum.

- Optical depth (μ): From a physical perspective, it describes how opaque the universe is at a given time seen from today at τ_0,

  $$\mu(\tau) \equiv \int_\tau^{\tau_0} \Gamma\left(\tau'\right) \mathrm{d}\tau'. \tag{25}$$

  It is important to note that this is a relevant factor since it establishes the probability of a photon not being scattered from τ until today, this being $e^{-\mu}$. This equation also implies that $\Gamma(\tau) = -d\mu/d\tau = -\dot{\mu}$ as it will be used later on.

- Visibility function (g): This function expresses the probability of a photon to last scatter at time τ as defined below,

  $$g = -\dot{\mu}e^{-\mu}. \tag{26}$$

  The explicit conformal time dependence is not specified in the visibility function as it will be also presented as g in the next steps of the derivation, but it is fully dependent on τ due to μ.

Now that these two concepts have been introduced, the derivation of the line-of-sight solution begins. The Boltzmann equation (23) can also be expressed as,

$$\frac{d\Theta}{d\tau} = \frac{d\ln\epsilon}{d\tau} - \Gamma\left[\Theta - \Theta_0 - \hat{\mathbf{n}}\cdot\mathbf{v}_e\right]. \tag{27}$$

Most of the terms in the above formula have already been introduced. The only term that is left to explain is

$$\frac{d\ln\epsilon}{d\tau} = -\frac{d\Psi}{d\tau} + (\dot{\Psi} + \dot{\Phi}), \tag{28}$$

which describes how the comoving energy ϵ evolves when metric perturbations are involved in the photon path. It is directly derived from General Relativity and sets the evolution of the photons 4-momemtum.

The factor $e^{-\mu}$ can be used as an integrative factor in the Boltzmann equation (27),

$$e^{-\mu}\frac{d\Theta}{d\tau} = e^{-\mu}\frac{d\ln\epsilon}{d\tau} + \dot{\mu}e^{-\mu}\left[\Theta - \Theta_0 - \hat{\mathbf{n}}\cdot\mathbf{v}_e\right]. \tag{29}$$

By moving the factor Θ from the right hand side of the equation to the left,

$$e^{-\mu}\frac{d\Theta}{d\tau} - \dot{\mu}e^{-\mu}\Theta = e^{-\mu}\frac{d\ln\epsilon}{d\tau} - \dot{\mu}e^{-\mu}\left[\Theta_0 + \hat{\mathbf{n}}\cdot\mathbf{v}_e\right]. \tag{30}$$

Working with the left hand side of the equation, the next total derivative can be used,

$$\frac{d}{d\tau}\left(e^{-\mu}\Theta\right) = e^{-\mu}\frac{d\Theta}{d\tau} - \dot{\mu}e^{-\mu}\Theta. \tag{31}$$

Therefore simplifying Eq. (30) to,

$$\frac{d}{d\tau}\left(e^{-\mu}\Theta\right) = e^{-\mu}\frac{d\ln\epsilon}{d\tau} - \dot{\mu}e^{-\mu}\left[\Theta_0 + \hat{\mathbf{n}}\cdot\mathbf{v}_e\right]. \tag{32}$$

Eq. (28) is now multiplied by the probabilistic factor, which can be used to introduce another total derivative in the following way,

$$e^{-\mu}\frac{d\ln\epsilon}{d\tau} = -e^{-\mu}\frac{d\Psi}{d\tau} + e^{-\mu}(\dot{\Phi}+\dot{\Psi}) = -\frac{d}{d\tau}\left(e^{-\mu}\Psi\right) - \dot{\mu}e^{-\mu}\Psi + e^{-\mu}(\dot{\Phi}+\dot{\Psi}), \tag{33}$$

since,

$$\frac{d}{d\tau}\left(e^{-\mu}\Psi\right) = e^{-\mu}\frac{d\Psi}{d\tau} - \dot{\mu}e^{-\mu}\Psi. \tag{34}$$

Therefore, the Boltzmann equation for scalar fluctuations can be expressed as,

$$\frac{d}{d\tau}\left[e^{-\mu}(\Theta+\Psi)\right] = g\left[\Theta_0 + \Psi + \hat{\mathbf{n}}\cdot\mathbf{v}_e\right] + e^{-\tau}(\dot{\Phi}+\dot{\Psi}), \tag{35}$$

or expressed with a source function $\hat{S}$ for convenience later on,

$$\frac{d}{d\tau}\left[e^{-\mu}(\Theta+\Psi)\right] = \hat{S}, \quad \text{where} \quad \hat{S} = g\left[\Theta_0 + \Psi + \hat{\mathbf{n}}\cdot\mathbf{v}_e\right] + e^{-\tau}(\dot{\Phi}+\dot{\Psi}). \tag{36}$$

3.3.2 Line-of-Sight Solution

Relating the temperature anisotropies at $\boldsymbol{x_0}$ in an arbitrary direction $\hat{\boldsymbol{n}}$ at τ_0 to the perturbation at recombination (spatially located at $\boldsymbol{x_*} = \boldsymbol{x}_0 + (\tau_0 - \tau_*)\,\hat{\boldsymbol{n}}$) can be done by solving the Boltzmann equation along the line-of-sight, i.e. integrating Eq. (36) from $\tau = 0$ until today τ_0,

$$\int_0^{\tau_0} d\tau \frac{d}{d\tau}\left[e^{-\mu}(\Theta+\Psi)\right] = \int_0^{\tau_0} d\tau \hat{S}\left(\tau, \vec{x}_0 + (\tau_0-\tau)\,\hat{n}, \hat{n}\right), \tag{37}$$

which can be expanded in the following way,

$$e^{-\mu(\tau_0)}\left[\Theta\left(\tau_0,\vec{x}_0\right) + \Psi\left(\tau_0,\vec{x}_0\right)\right] - e^{-\mu(0)}\left[\Theta\left(0,0\right) + \Psi\left(0,0\right)\right] = \int_0^{\tau_0} d\tau \hat{S}\left(\tau, \vec{x}_0 + (\tau_0-\tau)\,\hat{n}, \hat{n}\right), \tag{38}$$

from which the first exponential is 1 since $\mu(\tau_0) = 0$ and the second one vanishes due to $\mu(0) = \infty$. This would leave two terms on the left hand side of the equality but the gravitational potential contribution from the monopole today does not directly contribute since it is not observable [8], therefore giving the simplified equation below,

$$\Theta\left(\tau_0, \hat{x}_0, \hat{n}\right) = \int_0^{\tau_0} d\tau \hat{S}\left(\tau, , \vec{x}_0 + (\tau_0-\tau)\,\hat{n}, \hat{n}\right). \tag{39}$$

3.3.3 Projection

In order to find the transfer function $\Theta_l(k)$ (recall it is needed for the computation of the power spectrum as shown in Eq. (21) a mapping from momentum space to harmonic space is needed. This can be done by taking the line-of-sight solution, performing a Fourier transform to move to k-space, and using a plane-wave expansion so that the momentum plane waves are expressed as a linear combination of spherical waves.

The derivation will start from the line-of-sight solution in Eq. (39) and working separately with the right and the left hand side (RHS and LHS respectively) for the sake of neatness. Starting with a Fourier transform on the RHS,

$$RHS: \qquad \hat{S}\left(\tau,,\vec{x}_0+(\tau_0-\tau)\,\hat{n},\hat{n}\right)=\int\frac{d^3\vec{k}}{(2\pi)^3}\hat{S}(\tau,\vec{k},\hat{n})e^{i(\tau_0-\tau)\vec{k}\cdot\hat{n}}e^{i\vec{k}\cdot\vec{x}_0}. \tag{40}$$

Since the velocity $\vec{v_e}$ is Fourier transformed as $\vec{v_e}(\vec{k}) = -iv_e\hat{k}$, the source term from Eq. (36) neglecting anisotropic stress ($\Phi = \Psi$) is,

$$\hat{S}(\tau,\vec{k},\hat{n})e^{i(\tau_0-\tau)\vec{k}\cdot\hat{n}}=\left[g(\tau)\left(\Theta_0(\vec{k},\tau)+\Phi(\vec{k},\tau)-i\hat{k}\cdot\hat{n}v_e(\vec{k},\tau)\right)+2e^{-\mu}\dot{\Phi}(\vec{k},\tau)\right]e^{ix\vec{k}\cdot\hat{n}}. \tag{41}$$

The next step would be to introduce a plane wave expansion which takes the following general form,

$$e^{i\mathbf{k}\cdot\mathbf{r}}=\sum_{\ell=0}^{\infty}(2\ell+1)(-i)^\ell j_\ell(kr)P_\ell(\hat{\mathbf{k}}\cdot\hat{\mathbf{r}}), \tag{42}$$

where i is the imaginary unit, $\mathbf{k}$ and $\mathbf{r}$ are the wave and position vector respectively, j_l is the spherical Bessel function and P_l is the Legendre polynomial. In this scenario the equation is,

$$e^{i(\tau_0-\tau)\vec{k}\cdot\hat{n}}=\sum_{\ell=0}^{\infty}(2\ell+1)(-i)^\ell j_\ell(k(\tau_0-\tau))P_\ell(\hat{\mathbf{k}}\cdot\hat{\mathbf{n}}). \tag{43}$$

A useful expression is related to the derivative of this expansion,

$$\frac{d}{d(\tau_0-\tau)k}e^{i(\tau_0-\tau)\vec{k}\cdot\hat{n}}=\sum_{\ell=0}^{\infty}(2\ell+1)(-i)^\ell j'_\ell(k(\tau_0-\tau))P_\ell(\hat{\mathbf{k}}\cdot\hat{\mathbf{n}}), \tag{44}$$

where the prime in the spherical Bessel function denotes the derivative with respect to $(\tau_0-\tau)k$. Introducing $\chi=\tau_0-\tau$ and using $\vec{k}=k\hat{k}$, the RHS after implementing the plane wave transformation is found as shown below,

$$\int\frac{d^3\vec{k}}{(2\pi)^3}\int_0^{\tau_0}d\tau\hat{S}(\tau,\vec{k},\hat{n})e^{i\chi\vec{k}\cdot\hat{n}}e^{i\vec{k}\cdot\vec{x}_0}=$$

$$=\int\frac{d^3\vec{k}}{(2\pi)^3}e^{i\vec{k}\cdot\vec{x}_0}\sum_{\ell=0}^{\infty}(2\ell+1)(-i)^\ell P_\ell(\hat{\mathbf{k}}\cdot\hat{\mathbf{n}})\int_0^{\tau_0}d\tau\left[g(\tau)\left[(\Theta_0+\Phi)j_l(k\chi)-v_e j'_l(k\chi)\right]+2e^{-\mu}\dot{\Phi}j_l(k\chi)\right],$$

For the approach being taken in this paper, instantaneous recombination at τ_* is assumed and therefore, the factor $e^{-\mu}$ and the visibility function g can be approximated using a delta function and a Heaviside function H,

$$e^{-\mu}=H(\tau-\tau_*),\quad g(\tau)=\delta_D(\tau-\tau_*), \tag{45}$$

the following solution is obtained,

$$=\int\frac{d^3\vec{k}}{(2\pi)^3}e^{i\vec{k}\cdot\vec{x}_0}\sum_{\ell=0}^{\infty}(2\ell+1)(-i)^\ell P_\ell(\hat{\mathbf{k}}\cdot\hat{\mathbf{n}})\left[(\Theta_0+\Phi)j_l(k\chi_*)-v_e j'_l(k\chi_*)+2\int_{\tau_*}^{\tau_0}\dot{\Phi}j_l(k\chi)d\tau\right],$$

where $(\Theta_0+\Phi)$ and v_e are evaluated at $(\tau_*,\vec{k})$ but it has been suppressed for neatness and $\chi_*=\tau_0-\tau_*$.

The RHS of Eq. (39) has now been expanded and, the same transformations should be applied to the LHS so that the equality holds. However, showing the explicit transformations on the LHS is not necessary since it

has been previously shown in Eq. (18) for the derivation of the power spectrum formula. Extracting $\mathcal{R}(\mathbf{k})$ and comparing both terms leads to the following expression,

$$\Theta_l(k) = (2l+1)\left[(\Theta_0+\Phi)j_l(k\chi_*) - v_e j_l'(k\chi_*) + 2\int_{\tau_*}^{\tau_0}\dot{\Phi}j_l(k\chi)d\tau\right]. \tag{46}$$

This is the first expression of this thesis that relates the solution to the coupled equations to the transfer function. The first term is the Sachs-Wolfe (SW) term which describes the temperature perturbation including the gravitational redshift aforementioned. The second term is known as Doppler term and accounts for the energy created by the moving electrons when scattering occurs[6]. The last term is the previously mentioned ISW contribution which accounts for the time evolution of the potentials and, since this approach works on an always matter-dominated universe, the potentials do not vary over time and therefore the ISW effect does not contribute to the transfer function. Here is where another approximation is introduced, this being the matter-dominated universe. Due to this reason, ISW term will be removed from further derivations. Therefore, the final equation for the transfer function needed for the computation of the power spectrum is,

$$\Theta_l(k) = (2l+1)\left[[\Theta_0+\Phi](\tau_*,\vec{k})j_l(k\chi_*) - v_e(\tau_*,\vec{k})j_l'(k\chi_*)\right], \tag{47}$$

where the explicit $(\tau_*,\vec{k})$ dependence has been recovered. This calculation of the transfer function is commonly known as *free-streaming* which, in this context, refers to the fact the adiabatic perturbations right from recombination are almost non-changing and *stream* to the present. This is of course of great relevance since this perturbations will appear as anisotropies in the CMB, which is in agreement with the observational evidence.

3.4 Damping Scale

In the derivation above, multiple approximations have been taken into account for a more simplified approach. In the *tight coupling* limit, the mean free path for scattering Γ is assumed to be zero, referred to as *perfect tight coupling*. Together with the instantaneous recombination condition earlier introduced, the solutions would not be sufficiently accurate since these two approximations have great influence on the power spectrum peaks.

If recombination occurs during a certain finite time period and the mean free path accurately describes the real behaviour of photons, a damping on the small scale fluctuations appears when considering the recombination epoch. For this reason, an approximate damping scale, known as Silk damping [7], is introduced with the following exponential form,

$$D(k) = e^{-(k/k_D)^2}, \tag{48}$$

with

$$\kappa_D^{-2} = 2x_s^2 + \sigma^2 x_{\text{rec}}^2 \quad \text{where} \quad x_s \equiv 0.6(\Omega_m h^2)^{1/4}(\Omega_b h^2)^{-1/2}a_{\text{rec}}^{3/4} \quad \text{and} \quad \sigma \approx 0.03 \tag{49}$$

3.5 Summary of Approximations

A list with the approximations used in this thesis is presented below.

- Two fluid approach for the description of the fluctuations.
- Neglection of Anisotropic stress.
- Simplification of the Thomson scattering effects via the tight coupling limit.
- Only scalar fluctuations are considered.

[6] This term does not greatly influence the transfer function but it is of relevance for polarization effects [3].

4 Perturbation Analysis

4.1 Anisotropy Spectrum

When the coupled set of fluid equations shown in Eq. (13) is solved, the Sachs-Wolfe and Doppler terms that are necessary for the transfer function Θ_l in Eq. (47) and therefore also for the power spectrum C_l are found.

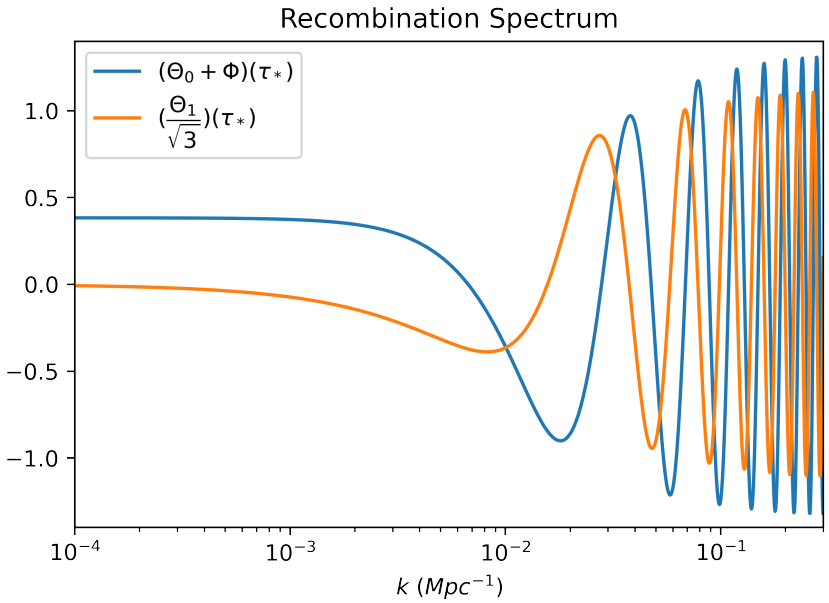

Figure 5: Sachs-Wolfe and Doppler terms evaluated at recombination conformal time τ_* for spectrum k

In Figure 5, the aforementioned terms are evaluated for a range of wavemodes k. The wavemode k is inversely proportional to physical scales/distance, therefore, when referring to large scales, it corresponds to small k wavemodes, and small scales to large k wavemodes. Both terms have oscillatory behavior on the small scales, differing slightly by a phase shift. To understand the meaning of these oscillations and the position of these peaks it is necessary to explicitely derive the oscillator equation that describes them.

The Boltzmann expression for the photon-baryon plasma from Eq. (23) can be separated into a set of two equations,

$$\dot{\Theta}_0 = -\frac{1}{3}k\Theta_1 + \dot{\Phi}, \tag{50}$$

$$\dot{\Theta}_1 = k\Theta_0 - k\Psi - \Gamma\left(\Theta_1 + v_\gamma\right). \tag{51}$$

These equations supplemented with the coupled fluid equations will lead to the desired oscillator equation. Rewriting the photon equations (13) in terms of multipole moments using Eq. (24) give the following formulas,

$$\dot{\delta}_\gamma = -kv_\gamma + 3\dot{\Phi}, \tag{52}$$

$$\dot{v}_\gamma = -\mathcal{H}v_\gamma - k\Psi - \frac{\Gamma}{R}\left(\Theta_1 + v_\gamma\right). \tag{53}$$

Applying the tight coupling limit, ($v_\gamma = -\Theta_1$), we find, after rearranging terms,

$$v_b \approx -\Theta_1 + \frac{R}{\Gamma}\left[\dot{\Theta}_{,1} + \mathcal{H}\Theta_1 - k\Psi\right], \tag{54}$$

which we substitute in Eq. (51) to obtain,

$$\dot{\Theta}_1 = -\mathcal{H}\frac{R}{1+R}\Theta_1 + \frac{k}{1+R}\Theta_0 - k\Psi. \tag{55}$$

Rearranging Eq. (50), Θ_1 can be obtained with a dependence only on Θ_0 and Φ terms,

$$\Theta_1 = \frac{-3}{k}\left[\dot{\Theta}_0 - \dot{\Phi}\right]. \tag{56}$$

Substituting into Eq. (55),

$$\dot{\Theta}_1 = -\mathcal{H}\frac{R}{1+R}\frac{-3}{k}\left[\dot{\Theta}_0 - \dot{\Phi}\right] + \frac{k}{1+R}\Theta_0 - k\Psi. \tag{57}$$

Taking a time derivative of Eq. (51), we find an expression for $\dot{\Theta}_1$,

$$\dot{\Theta}_1 = \frac{-3}{k}\left[\ddot{\Theta}_0 - \ddot{\Phi}\right]. \tag{58}$$

Comparing Eqs. (57) and (58), the following oscillator equation can be obtained,

$$\ddot{\Theta}_0 + \mathcal{H}\frac{R}{1+R}\dot{\Theta}_0 + c_s^2 k^2 \Theta_0 = -\frac{1}{3}k^2\Psi + \ddot{\Phi} + \mathcal{H}\frac{R}{1+R}\dot{\Phi}, \tag{59}$$

where c_s is the sound speed of the coupled photon-baryon fluid,

$$c_s^2 \equiv \frac{1}{3(1+R)}. \tag{60}$$

The oscillatory equation (59) relates the physical effects occurring on the CMB to the temperature monopole. The solutions to this equation will be dependent on the scales, in other words, the temperature perturbations have different behaviour on the physical distance being considered. The solutions to equation produces *acoustic oscillations*, already presented in Figure 5. A derivation of the analytical solutions and the explanation of the physics behind will be described in the next subsection.

4.2 Acoustic Oscillations

The acoustic oscillator equation can be reduced to a simple harmonic oscillator from which analytical solutions can be obtained. The transformation from Eq. (59) to its simplified form is achieved by assuming that the rate of change of the potential Φ and of R over time is minimal compared to the oscillation frequency $\omega = c_s k$, if it were to be expressed as a simple harmonic oscillator. These assumptions lead to the following equation,

$$\ddot{\Theta}_0 + c_s^2 k^2 \Theta_0 = -\frac{k^2}{3}\Psi. \tag{61}$$

The term $c_s^2 k^2 \Theta_0$ can be interpreted as the photon pressure since it is directly dependent on Θ_0 and the $-\frac{k^2}{3}\Psi$ term as a gravitational forcing term. The solution to this equation, using the adiabatic initial condition that $\dot{\Theta}_0(0, \mathbf{k}) = 0$, is

$$\Theta_0(\tau, \mathbf{k}) = [\Theta_0(0, \mathbf{k}) + (1+R)\Psi(\mathbf{k})]\cos(kr_s) - (1+R)\Psi(\mathbf{k}), \tag{62}$$

where the sound horizon has been introduced using,

$$r_s = \int_0^\tau c_s \, \mathrm{d}\tau'. \approx c_s \tau. \tag{63}$$

In the limit $R \to 0$, which would correspond to a time where photons dominated, the solution would be the expression of a harmonic oscillator with a shift due to the gravitational potential Ψ,

$$\Theta_0(\tau, \mathbf{k}) = [\Theta_0(0, \mathbf{k}) + \Psi(\mathbf{k})]\cos(kr_s) - \Psi(\mathbf{k}). \tag{64}$$

The redshift and blueshift effects related to the gravitational potential mentioned earlier in Section 3.3 appear in this solution. If $-\Psi(\mathbf{k}) > 0$, the density of photons described by Θ_0 would increase inside the potential well as well as introducing a blueshift effect on the photons, therefore raising their temperature. Nevertheless, the pressure exerted by the compressed fluid inside the well causes this potential barrier to flatten. While this process is occurring, photons decouple from the fluid and loose energy on exit, which can be referred to as a

redshift. This essentially cancels the blueshift due to $-\Psi(\mathbf{k})$, therefore, the observed temperature fluctuation takes the following form,

$$\Theta_0(\tau, \mathbf{k}) + \Psi(\mathbf{k}) = [\Theta_0(0, \mathbf{k}) + \Psi(\mathbf{k})] \cos(kr_s). \tag{65}$$

From this, it is obvious that all the Fourier modes will have a the same phase when recombination conformal time τ_* is reached, in other words, the fluctuations are temporally coherent [13]. This is really when a mechanism that produces fluctuations with the same phase and have supposedly never been in causal contact is needed. This mechanism is inflation, producing coherent fluctuations. There will be a selected set of wavemodes that produce maximum and minimum temperature contributions at decoupling, these being,

$$k_n = \frac{n\pi}{r_s}. \tag{66}$$

The extrema produced by these specific modes of oscillation correspond to the peaks observed in the power spectrum. In this last derivation, the effects of the baryons have not been considered in the fluid. The temperature anisotropies would be influenced by the effects introduced by this particle species, since the sound speed c_s would change, and so would the behaviour between pressure and the gravitational forcing. The introduction of baryons in the acoustic oscillations is known as *baryon loading*. The fluid would be more compressed in the potential wells and therefore implementing a shift from its zero-point oscillation,

$$\Theta_0(\tau, \mathbf{k}) + \Psi(\mathbf{k}) = [\Theta_0(0, \mathbf{k}) + \Psi(\mathbf{k})] \cos(kr_s) - R\Psi(\mathbf{k}). \tag{67}$$

This gravitational term can be interpreted as an increase in the fluctuation due to the load of baryons. This compresses the fluid in the potential well while peaks with reduced density, these being the *potential hills*, will not be enhanced. This effect is not of great relevance in this approach, since $R \to 0$ at early times.

From Eq. (50) for the photon-baryon fluid, the solution to the dipole term is,

$$\Theta_1(\tau, \mathbf{k}) = -3\,[\Theta_0(0, \mathbf{k}) + (1+R)\Psi(\mathbf{k})]\, c_s \sin(kr_s). \tag{68}$$

Notice the c_s factor involved. This expression can be rearranged, this being the reason why it is common to plot the dipole term over a factor of $\sqrt{3}$. Now that the acoustic oscillator equation has been analyzed in detail, the recombination spectrum shown in Figure 5 is easier to comprehend.

In the low scale regime, corresponding to large values of k, the observed perturbation is highly oscillating, which corresponds with the potential wells and hills earlier described. Notice that for every maximum peak on $(\Theta_0 + \Psi)$, which would correspond to a high density area in the fluid, its velocity described by Θ_1 is in range close to 0, thus implying that the fluid is not moving or escaping the potential well. The same analysis can be done on the zero-point of $(\Theta_0 + \Psi)$ at which Θ_1 is maximum due to the photons decoupling exiting the perturbations. Looking at the small k regime, both terms acquire a constant value. This is due to the extremely large scales being considered, usually known as super-Hubble modes, at which the perturbations have not been able to propagate yet.

Even though the approximation of matter-dominated Universe is being considered in Section 3.3.3, it is only used in the free-streaming derivation. To clarify this, it has to be understood that the Universe underwent a series of eras in which the different contributors to the metric dominated. The early Universe first went through the radiation era, in other words, the electromagnetic radiation dominated over the matter density. Afterwards, it transitioned to the matter dominated era, mentioned earlier in this thesis by the introduction of a_{eq}, which is the expansion factor at equality defined as the time where this transition occurred and both the radiation and matter density had equal contributions. Then, it transitioned into the dark energy era, being the current state of the Universe. When it is said that the matter-dominated approximation is being used, it is assumed that the Universe did not transition into the dark energy era so that the ISW effect in Eq. 46 can be neglected.

Nevertheless, the matter-dominated approximation is only applied to the ISW term in the transfer function but not in the evolution of the coupled equations or in the acoustic oscillation description. In the radiation era, the gravitational potentials vary inside the horizon [1] as shown in Figure 6.

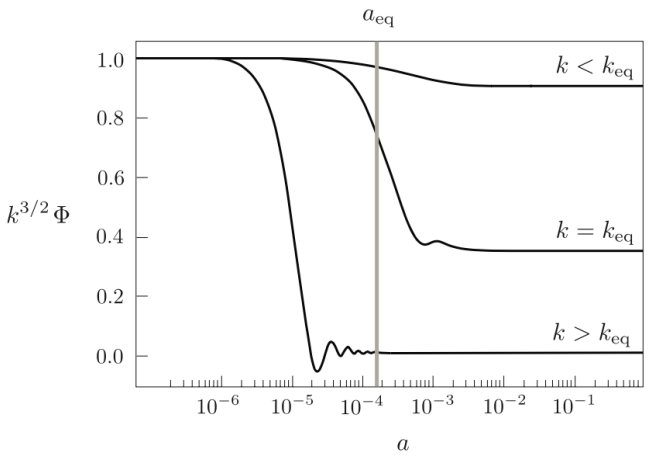

Figure 6: Solutions for the linear evolution of the gravitational potential (figure adapted from [1])

The decay of the potential after sound horizon crossing is due to radiation itself. The gravitational potential is created by the radiation itself since it is the dominant density, this relationship is given by relativistic form of the Poisson equation,

$$\nabla^2\Phi - 3\mathcal{H}(\dot{\Phi} + \mathcal{H}\Psi) = 4\pi G a^2 \delta\rho, \tag{69}$$

where $\delta\rho$ is the total density perturbation given by $\delta\rho \equiv \sum_a \delta\rho_a$ and G is Newton's gravitational constant. For this derivation, modes inside the Hubble radius are considered, which expressed in Fourier space correspond to $k \gg \mathcal{H}$, leading to the following equation,

$$\nabla^2\Phi \approx 4\pi G a^2 \delta\rho. \tag{70}$$

Pressure impedes the radiation from compression in the potential well, constraining the density fluctuation to acquire a constant value, thus, from Eq. (70), the potential decays. Since the decay occurs in the fully compressed stated, the fluid is allowed to oscillate with no resistance from the any gravitational potential, making the amplitude of the oscillations grow large. This effect is known as *radiation driving* and its physical implications on the power spectrum will be later addressed.

5 Cosmological Boltzmann Code

The treatment given to the formulas and derivation previously explained is fully analytical. The adaptation of the analytical equations into a Python code requires specification of integration methods, limits and modifications needed for computational purposes. The code can be found in a GitHub repository [9].

5.1 Approach

The code has been written such that variation of the different parameters is possible, with that determining other initial variables. Changes in the variables and the calculation of the other initial quantities is done through the function *init_params* after inputting the desired conditions.

The computation of the power spectrum is done through the function *power_spectrum* which takes as input a list containing the range of l values and returns a list containing the values of $l(l+1)C_l$. This function solves the coupled equations presented in Eq. (13) therefore getting the monopole and dipole solutions show in Eq. (24) for all the k-spectrum evaluated at recombination.

Once the equations of motion are solved, using these solutions into the the transfer function from Eq. (47), implementing the damping and the primordial power spectrum from Eqs. (48) and (22) respectively, and integrating as shown in Eq. (21) gives the desired final result. If the goal of the computation is to obtain a graph of the power spectrum for different values of a certain parameter, *init_params* should be executed before the power spectrum is calculated for every value of the varying parameter since the change of one density affects all the other initial parameters involved in the equations. A more detailed overview of the methods used can be found in the next section.

5.2 Parameter Definition

The code is functional when provided with a set of initial conditions, those being the densities for the different contributors, these being:

- The matter density Ω_m, dependent on both the baryonic density Ω_b and on the CDM density Ω_c as,

$$\Omega_m = \Omega_b + \Omega_c. \tag{71}$$

- The curvature density Ω_k, which describes the curvature of the cosmological model being considered (For a flat universe, $\Omega_k = 0$).
- The dark energy density Ω_{de}, associated with the dark energy or cosmological parameter Λ.
- The radiation density Ω_r which has the following equation,

$$\Omega_r = f_\nu \Omega_\gamma, \tag{72}$$

  where f_ν is the neutrino fraction and Ω_γ is the photon density.

All of these densities much satisfy that their sum has to be equal to a total density Ω_0 which is set to be 1,

$$\Omega_0 = \sum_i \Omega_i = \Omega_m + \Omega_r + \Omega_k + \Omega_{de} = 1 \tag{73}$$

With these relations one can vary the desired parameter with ease. The only other parameter that can be varied from the code through *init_params* is is h, the reduced Hubble parameter. If desired, any other initial condition contained in *init_params* can be varied with a simple modification to the code.

Conformal time τ is of relevance for the computations and it can be calculated using the following relationship,

$$\tau(a) = \int_0^a da' \frac{1}{a'^2 H_0 \sqrt{\Omega_r (a')^{-4} + \Omega_m (a')^{-3} + \Omega_k (a')^{-2} + \Omega_{de}}}. \tag{74}$$

As shown above, it can be described using a dependence on the cosmological densities, therefore changing when these parameters are varied. The conformal time at recombination τ_* is usually needed for the computation of

other equations and it can be found by substituting the upper bound of the integral by the desired expansion factor a_*. The conformal time today τ_0 can therefore be found by using $a_0 = 1$.

It is common to use the redshift z to refer to the scale factor a or to conformal time τ. A simple formula that relates these variables,

$$a(z) = \frac{1}{1+z}. \tag{75}$$

Since the redshift at recombination z_* is known, the scale factor a_* can be easily calculated.

5.3 Initial Conditions

The values for the cosmological variables do not have to exactly match the ΛCMD model since the purpose of this paper is to study the variation of the power spectrum for the changes on these parameters. The values used are presented in this subsection.

5.3.1 Cosmological Parameters

The values chosen as initial conditions for a better representation of the perturbation graphs and for the power spectrum computation are,

	Symbol	Value
Densities	Ω_b	0.053
	Ω_m	0.229
	Ω_k	0
	Ω_{de}	0.7709
	Ω_γ	5.04×10^{-5}
Other Parameters	h	0.7
	f_ν	1.68
	z_*	1100
	k_{pivot}	0.05
	A_s	2.2×10^{-9}
	n_s	0.967

Table 1: Parameter values assigned for the computation of the power spectrum.

5.3.2 Coupled Fluid Equations Revisited

The coupled equations of motion have to be supplied with initial conditions for them to be solvable, these are:

$$\begin{aligned} \delta_\gamma &= -2\Phi, \\ \delta_c &= \frac{3}{4}\delta_\gamma, \\ v_\gamma &= -\frac{1}{4}\frac{\kappa}{\eta}\delta_\gamma, \\ v_c &= v_\gamma. \end{aligned} \tag{76}$$

Notice the dependence of all the parameters on the initial gravitational potential Φ. The choice of this parameter may vary depending on the approach being considered. For the approach being treated in this paper, $\Phi = 1$, due to the fact that this setting allows the extraction of the primordial curvature perturbation $\mathcal{R}(\mathbf{k})$ from the transfer function.

5.4 Adaptation of Equations and Integration Methods

5.4.1 Multipole Computation

The computation of the power spectrum requires the integration of the transfer function, in other words, the solution to the fluid equations at recombination for all the k-spectrum is needed. Since the integration would

take too much computational time if it were to solve the fluid equations for each k-value, the fluid equations are first solved and then interpolated.

The goal of this multipole computation is to evolve the fluid equations till recombination for all the k-space. To solve Eq. (13) with *scipy.integrate.odeint*, a specification of a time range and a κ range is necessary. These functions have been rescaled as in the coupled equations shown in Eq. (13), therefore using κ instead of k or l. The range of values for the rescaled wavemodes is chosen to be $10^{-2} < \kappa < 10^{3}$ in logspace, which can be associated with k approximately going from $10^{-4} < k < 1\ Mpc^{-1}$. The rescaled time x range is chosen to be $10^{-6} < x < x_*$, with x_* being the rescaled conformal time at recombination calculated using Eq. (74) with a_* and rescaling with τ_r.

With the above defined limits, the fluid equations are solved for the full k-space being considered. The only contributors that are of interest for the computation of the transfer function, as shown in Eq. (47), are the SW term and the Doppler term, these being $[\Theta_0 + \Phi]$ and Θ_1. Expressed with the fluid equations notation, these terms are $\left[\frac{1}{4}\delta_\gamma + \Phi\right]$ and $-v_\gamma$. These solutions are separated and interpolated over the κ range, for a faster but accurate computation of the transfer function Θ_l.

5.4.2 The Transfer Function and Power Spectrum Revisited

The power spectrum calculation requires the square of the transfer function inside of the integral as shown Eq. (21). The transfer function from Eq. (47) has two terms after neglecting the contribution from the ISW term, therefore, squaring it would lead to an expression with 3 terms, one of them being the product of the SW and Doppler term. This cross term can also be neglected since its contribution is minimal compared to the square of the monopole and dipole terms in Θ_l [3]. Therefore, the transfer function squared would take the following form,

$$\Theta_l(k)^2 \approx (2l+1)^2 \left[\left[\Theta_0 + \Phi\right]^2 (\tau_*, \vec{k}) j_l^2(k\chi_*) + v_e^2(\tau_*, \vec{k}) j_l'^2(k\chi_*) \right]. \tag{77}$$

Substituting this into the power spectrum expression from Eq. (21) and simplifying,

$$C_l = 4\pi \int \mathrm{d}\ln k \ \left[\left[\Theta_0 + \Phi\right]^2 (\tau_*, \vec{k}) j_l^2(k\chi_*) + v_e^2(\tau_*, \vec{k}) j_l'^2(k\chi_*) \right] \Delta^2_{\mathcal{R}}(k). \tag{78}$$

Note that the power spectrum is given by C_l, and the expression on the RHS is k and τ dependent. Therefore, it would be of convenience to modify this integral so that it is an expression dependent on rescaled time x and on l. Recall $l \approx (k_* [\tau_0 - \tau_*])$, using $k = xk_*$, two expressions can be obtained, one for κ which is involved in the monopole and dipole terms, and for $k_* [\tau_0 - \tau_*]$ involved in the spherical Bessel functions,

$$\kappa = k\tau_r = xk_*\tau_r = xl\frac{\tau_r}{\tau_0 - \tau_*},$$

and

$$k_* [\tau_0 - \tau_*] = x\frac{l}{\tau_0 - \tau_*}(\tau_0 - \tau_*) = xl,$$

Therefore, the power spectrum takes the following form in the code,

$$C_l = 4\pi \int \frac{\mathrm{d}x}{x} \left[\left[\Theta_0 + \Phi\right]^2 \left(xl\frac{\tau_r}{\tau_0 - \tau_*} \right) j_l^2(xl) + v_e^2 \left(xl\frac{\tau_r}{\tau_0 - \tau_*} \right) j_l'^2(xl) \right] \Delta^2_{\mathcal{R}} \left(\frac{xl}{\tau_0 - \tau_*} \right) D \left(\frac{xl}{\tau_0 - \tau_*} \right). \tag{79}$$

Note that the differential is changed and it is now x dependent, which is desired to take into account the free-streaming of the perturbations till today. Also note the addition of the damping scale previously introduced in Eq. (48) and its change of variable.

All the equations earlier derived referring to the monopole and dipole terms have been given k dependence instead of κ. The change represented in this last equation takes into account that the monopole and dipole take κ as an argument, which is the treatment given in the code since the solutions to the fluid equations are rescaled.

5.4.3 Spherical Bessel Functions

The mapping between the wavemodes k in Fourier space to the multipole moment l of the spherical harmonics is possible only thanks to the Bessel functions in its spherical form. This is only approximately true, since the mapping is done correctly at $l \approx (k_* [\tau_0 - \tau_*])$ where the Bessel function peaks.

In the equations used, the spherical Bessel function is always involved in its squared form which has the following behaviour,

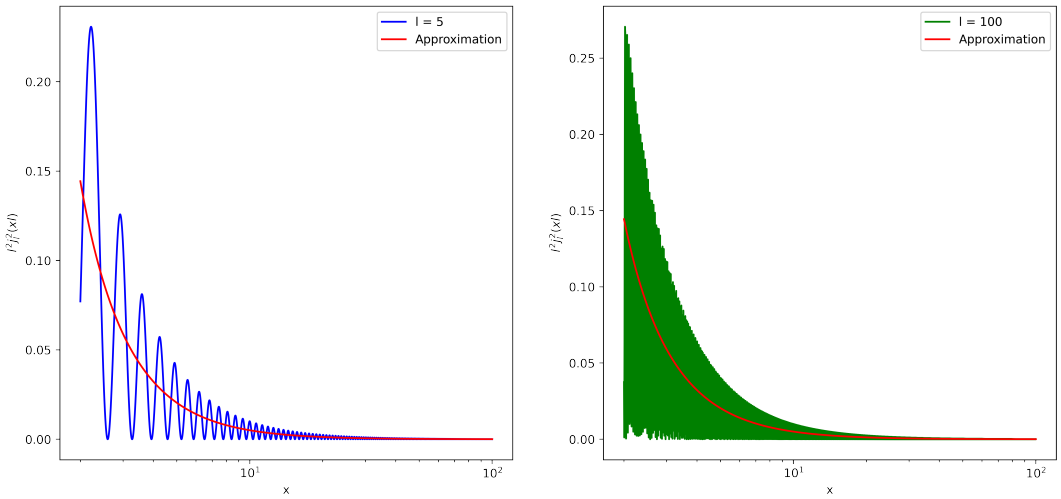

Figure 7: Spherical Bessel function plotted for two values of l and using the approximation for large x and xl

In Figure 7, the highly oscillating behaviour of the Bessel functions is plotted. The equation for the spherical Bessel function,

$$j_l(x) = \sqrt{\frac{\pi}{2x}} J_{l+1/2}(x), \tag{80}$$

where J_l is the ordinary Bessel function. To understand this oscillating pattern in the limit where both x and xl are large, a modification of $J_l(x)$ is required since it contains both variables. For the large limit being considered in this scenario, it is possible to express the ordinary Bessel function from the dominant term in the Meissel series expansion [6],

$$J_\nu(x) \simeq \sqrt{\frac{2}{\pi\sqrt{x^2 - v^2}}} \cos\left(Q_\nu(x) - \tfrac{1}{4}\pi\right) \quad \text{with} \quad Q_\nu(x) = \sqrt{x^2 - v^2} - \tfrac{1}{2}v\pi + v \arcsin(v/x). \tag{81}$$

Substituting this back into the spherical Bessel function with xl as the argument of the function gives,

$$j_l(xl) \simeq \sqrt{\frac{\pi}{2xl}} \sqrt{\frac{2}{\pi\sqrt{x^2 l^2 - \left(l + \frac{1}{2}\right)^2}}} \cos\left(Q_{l+1/2}(xl) - \frac{1}{4}\pi\right). \tag{82}$$

Since the spherical Bessel function present in the equations is squared and multiplied by a factor of l^2, after simplifying the following expression is obtained,

$$l^2 j_l^2(lx) \simeq \frac{1}{x\sqrt{x^2 - \left(\frac{2l+1}{2l}\right)^2}} \cos^2\left(Q_{l+1/2}(xl) - \frac{1}{4}\pi\right). \tag{83}$$

From this final equation, a rather simple but useful approximation can be done. By approximating the cosine term by its average, $1/2$, and approximating $\left(\frac{2l+1}{2l}\right)^2 \simeq 1$ in the large l regime, the complete approximation for the spherical Bessel function is,

$$l^2 j_l^2(xl) = \frac{1}{2x\sqrt{x^2-1}}, \tag{84}$$

with its derivative being,

$$l^2 j_l'^2(xl) = \frac{1}{2x\sqrt{x^2-1}} \frac{x^2-1}{x^2}. \tag{85}$$

These two equations are used in the code for the computation of the integrals required for the power spectrum. As it can be seen from Figure 7, the approximation does well averaging the peaks and it can be integrated with ease compared to the original high oscillating spherical Bessel functions.

5.4.4 Polishing The Power Spectrum

The implementation of the spherical Bessel functions approximations into the power spectrum requires Eq. (79) to be multiplied by a factor of l^2, so that the Bessel functions also pick up this term. Before introducing this factor, it is easy to notice from Figure 5 that the SW term remains constant in super-Hubble modes at recombination while the Doppler term vanishes. This leads to an equation of the power spectrum which is only dependent on the monopole term,

$$C_l \approx C_l^{SW} = 4\pi \int \frac{\mathrm{d}x}{x} \left[[\Theta_0 + \Phi]^2 \left(xl \frac{\tau_r}{\tau_0 - \tau_*} \right) j_l^2(xl) \right] \Delta_{\mathcal{R}}^2 \left(\frac{xl}{\tau_0 - \tau_*} \right), \tag{86}$$

where the damping scale has not been added to the equation since it does not affect the perturbations at super-Hubble modes. With a scale-invariant expectation value of the primordial curvature perturbations $\Delta_{\mathcal{R}}^2 = A_s$, the above equation takes the following form,

$$C_l \to \frac{4\pi}{25} A_s \int \mathrm{d} \ln x j_l^2 (xl) \,. \tag{87}$$

When using the integral shown below,

$$\int_0^\infty \mathrm{d} \ln x j_l^2(x) = \frac{1}{2l(l+1)}, \tag{88}$$

gives the power spectrum C_l constant value,

$$l(l+1) C_l = \frac{4\pi}{25} A_s. \tag{89}$$

This is of great relevance since it implies that the low-l regime of the spectrum being considered C_l will have a constant value, therefore allowing for an estimation of A_s and most importantly, the determination of the full expression of $\Delta_{\mathcal{R}}^2$.

This is the reason why the power spectrum is commonly plotted as $l(l+1)C_l$, so that it provides information about the nature of the primordial curvature perturbation. For the purpose of this derivation and for the approximations of the spherical Bessel function considered in this paper, the factor $l(l+1)$ can be approximated to l^2, allowing the use of the approximations aforementioned. To conclude, the full equation that computes the power spectrum in the code is,

$$l^2 C_l = 4\pi \int \frac{\mathrm{d}x}{x} \left[[\Theta_0 + \Phi]^2 \left(xl \frac{\tau_r}{\tau_0 - \tau_*} \right) l^2 j_l^2(xl) + v_e^2 \left(xl \frac{\tau_r}{\tau_0 - \tau_*} \right) l^2 j_l'^2(xl) \right] \Delta_{\mathcal{R}}^2 \left(\frac{xl}{\tau_0 - \tau_*} \right) D \left(\frac{xl}{\tau_0 - \tau_*} \right). \tag{90}$$

5.5 Capability

The code used for the calculation of the power spectrum uses the equations derived in this thesis. Computation of the spectrum using *power_spectrum* for a set of given initial parameters calculated with *init_params* takes approximately 1 minute. The variation of the parameters presented in the following section requires different *init_params* functions in certain cases as the other densities had to be calculated using the relationships shown in Section 5.2. The code is simple enough to be manipulated to add new contributions if a more accurate approach is desired.

6 Heights of the Peaks

The dependence of the power spectrum on the multiple cosmological parameters is somewhat intricate, therefore, a brief explanation of the various peaks is developed below. As shown in Section 3.3, the spatial inhomogeneities at recombination conformal time τ_* are mapped to angular anisotropies, thus, when inspecting the power spectrum, one is directly observing the fluctuations from inflation itself. Briefly discussed in Section 4.2, the extrema of the acoustic oscillations are represented as peaks in the CMB power spectrum, all part of a harmonic series that manifests the physical processes the early universe plasma underwent. The power spectrum for the initial conditions set in Section 5.3.1 is presented in Figure 8.

A useful way to understand the meaning of these peaks and their angular location is to think about the photons travelling towards the observer after decoupling. The first photons that arrive would be the ones leaving the gravitational potential first and, as time progresses, more photons would reach the observer, all of them leaving at a later time the perturbations and therefore undergoing multiple compressions and rarefications in the plasma. Thus, the first peak corresponds to the mode that was compressed once, the second peak to the mode that was compressed and then rarefied, etc. Exploiting this concept, a correlation between the angular location l of the peaks and the curvature of the universe can be made since it would determine how much distance the photons had to travel to reach the observer. The first peak is located at $l \sim 200$ which corresponds to a spatially flat universe [15]

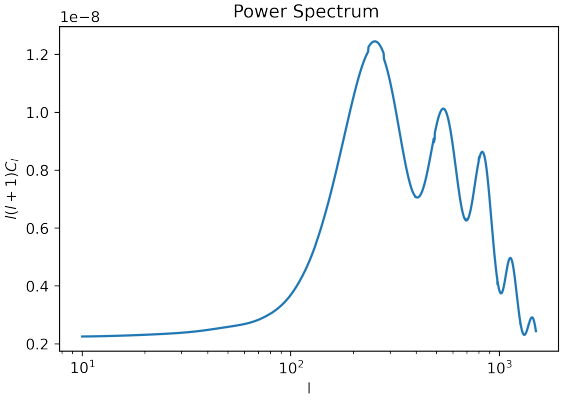

Figure 8: Power spectrum for fixed initial conditions

The baryon loading concept introduced in Section 4.2 shall be recovered here, as it is useful to comprehend the behaviour of the first and next peaks. Baryons add pressure to the plasma trapped in the potential wells and thus, when photons decouple, they exit the potential with greater energy than if the baryons were not present in the fluid. The height of the first peak, which as explained above represents the mode that has been compressed only once, is directly influenced by the amount of baryons in the fluid. This can be generalized to all the odd peaks in the power spectrum since they are associated with the compression of the fluid. The matter density also influences the height of this first peak since matter accounts for both baryonic and cold dark matter. The height of the higher peaks is therefore influenced by these two parameters. These two densities are the main source of modification of the power spectrum when manipulated. Other parameters have influence in the formation of the peaks but the shape is mostly maintained.

The almost flat regime of the power spectrum, located in the lower angular scale l, represents the plateau described in Section 5.4.4, which essentially corresponds to the almost constant behaviour of the SW and Doppler terms in the recombination spectrum shown in Figure 5.

6.1 Parameter Variation

Various cosmological parameters will now be varied in order to see their effects on the power spectrum. This allows a better understanding of the physical events and how the power spectrum would be modified depending on the cosmological model being considered. As shown in the figures presented below, the CMB angular power spectrum is sensitive to changes in its parameters. The peaks exhibit similar behavior to variations of distinct parameters, which is known as parameter degeneracy.

6.1.1 Hubble Parameter

The reduced Hubble parameter h, which obviously refers to the expansion of the universe, sets the height of the peaks since it constrains the distance photons have to travel to reach the observer after decoupling. This parameter is varied in the Figure below.

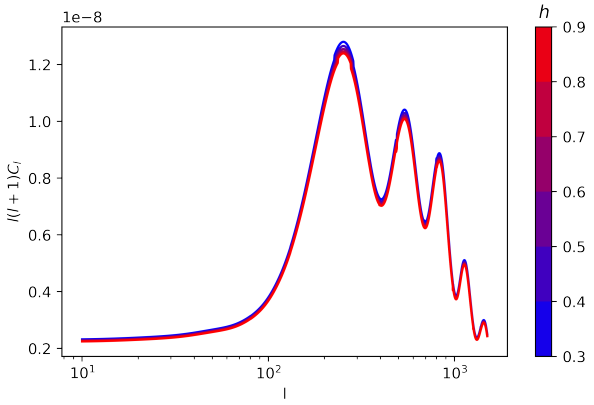

Figure 9: Power spectrum for multiple values of the reduced Hubble parameter h

The higher h is, the faster the universe expands, thus forcing the photons to travel more distance and loosing more energy on the process, lowering the temperature anisotropies. The same reasoning is applied to the lower range of h values being considered, therefore expecting higher temperature fluctuations.

6.1.2 Dark Energy Density

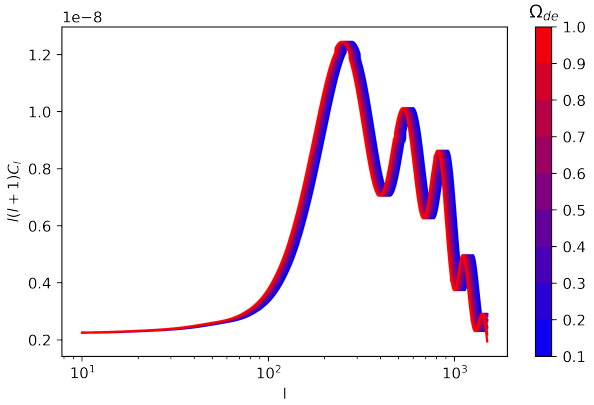

Figure 10: Power spectrum for multiple values of the dark energy density Ω_{de}

The dark matter energy density is only explicitly involved in Eq. (74), thus, when this parameter is changed, only the conformal time at recombination τ_* varies. The larger Ω_{de} is, the earlier recombination occurs therefore shifting all the power spectrum to the right since the photons reach the observer earlier.

6.1.3 Baryon Density

Considering multiple baryon density Ω_b values, Figure 11 is obtained. The change of the first peak height is noticeable for the range of values being considered. This is essentially the extra pressure on the potential well due to the additional baryons, thus, an increase in height is expected for increasing baryon density.

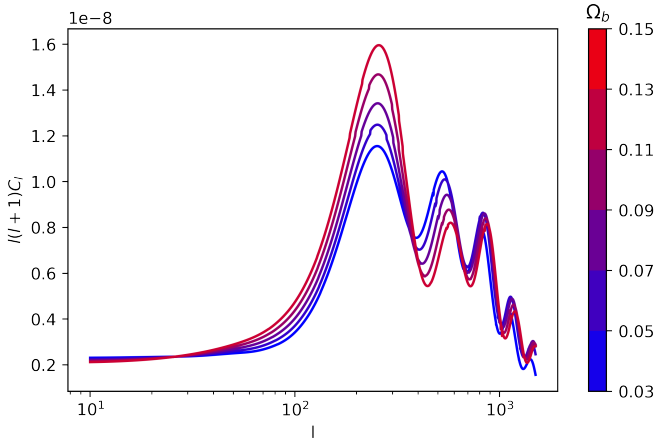

Figure 11: Power spectrum for multiple values of baryonic density Ω_b

The reduction in the second peak while maintaining the height of the third peak is due to the almost constant rarefication of the fluid despite the additional baryonic matter.

6.1.4 Matter Density

The physics behind the third peak of the power spectrum can be studied by varying the matter density Ω_m as shown in Figure 12. In the model being used, the baryon density Ω_b is fixed to the initial condition shown in Table 1, which implies from Eq. (71) that the CDM density Ω_c is the variable being changed. The behaviour of the peaks is almost contrary to the variation of the baryon density as the overall power spectrum is rescaled down when the matter density is increased.

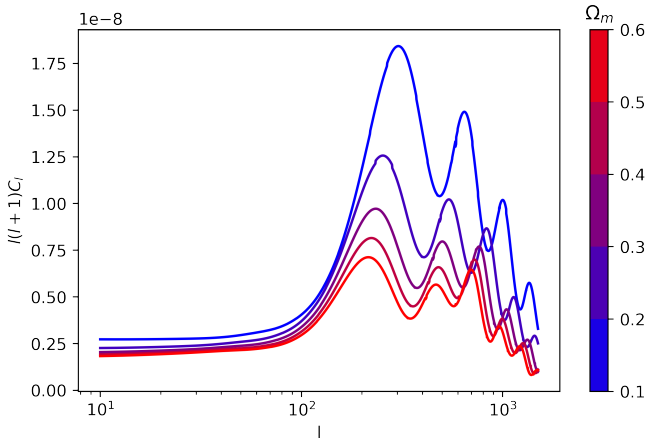

Figure 12: Power spectrum for multiple values of matter density Ω_m

A reduction on the second peak can be observed for high values of matter density, similiar effect to the observed in the baryon density variation. However, for low values of matter density, an overall increase of the peaks occurs, contrary to the amplification of only the odd peaks seen in Figure 11. The behavior of the peaks can be explained by looking at the matter-radiation equality defined in Section 3.1 as $z_{eq} = a_{\text{eq}}^{-1} \approx 2.4 \times 10^4 \Omega_m h^2$. From this, it can be inferred that for lower values of Ω_m, z_{eq} will decrease, meaning that the matter-radiation equality will be shifted to later times, closer to recombination. This fact implies that the radiation era lasted longer and, due to the oscillations in the radiation era introduced in Section 4.2, the amplified oscillations due to radiation driving would be the observed peaks of Figure 12.

For greater values of Ω_m, the CDM density increases due to the baryon density being fixed. With the thought process above discussed, the matter radiation equality would be shifted to earlier times and therefore the driving

effect disappears, thus reducing the amplitudes. The additional dark matter contributes to the rarefication in the same way as baryons do, thus the second peak is reduced. However, a reduction of the first peak is observed, contrary to the rise found with baryon loading. Since the amount a baryons is not increased, there are not so many photons decoupling, also lowering the height of the first peak.

6.1.5 Curvature

As explained in the beginning of this section, the angular position of the peaks can be used to determine the curvature of the universe. Therefore, varying the curvature density Ω_k should shift the power spectrum to higher or lower values of l.

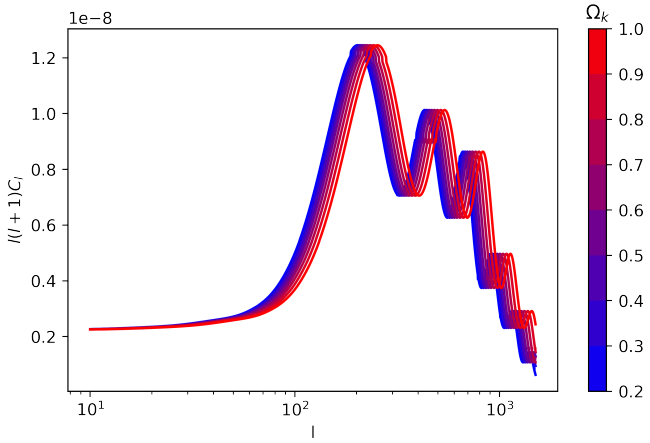

Figure 13: Power spectrum for multiple values of curvature density Ω_k

The higher the value of Ω_k, the more to the right the power spectrum is shifted. This effect is due to the greater distance that the photons would have to travel for higher curvature density.

7 Conclusion

7.1 Accuracy

The two fluid approach being considered in this thesis, as well as other approximations implemented, produce an angular power spectrum which correlates with the acoustic oscillations and the physical processes that the universe underwent.

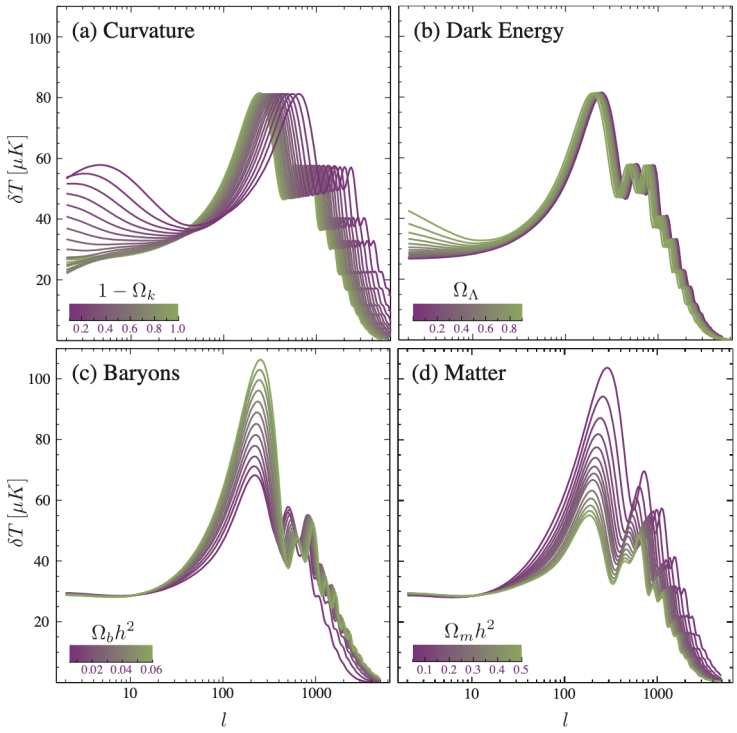

Figure 14: Power spectrum varied for multiple cosmological parameters (figure adapted from [14])

Comparing the figure above, which represents the analytical solution, to the graphs developed with the two fluid approximation, clearly shows that the toy-model being considered reproduces to great accuracy the power spectrum. The curvature density graph differs in the large scale limit from Figure 13. This is due to the ISW effect not being considered in the approach of this thesis. However, the shift of the power spectrum over the angular scale matches with great precision Figure 14. The dark energy variation of the power spectrum is matches to great precision Figure 14 except for large scale solutions. This is again due to the ISW being neglected in the approach taken. The figures representing the variation of the baryon density show an identical power spectrum. The matter density alteration produces a power spectrum which also matches the graph from Figure 14 although with small differences, but overall very much alike.

7.2 Summary of Main Contributions

Although there are small differences in the power spectrum when considering parameter variation, the two fluid approach considered successfully reproduces the evolution of the inhomogeneities and therefore, temperature anisotropies are described to great accuracy. This thesis not only provides the reader with the physical background required for the complete understanding of the formation of the power spectrum, but also presents the full equation derivation in addition to a simple, yet powerful Python code.

7.3 Future Work

A detailed analysis of the peak behavior of the power spectrum could determine to great accuracy the various cosmological parameters in the two fluid approximation. This could be compared to other models so that better approximations or extra modifications can be implemented, therefore reaching an even more accurate computation and understanding of the physics behind the CMB temperature map.

Bibliography

[1] D. Baumann, *Advanced Cosmology* (Lecture notes). University of Amsterdam.

[2] D. Baumann, *Cosmology Part III*. University of Amsterdam.

[3] D. Baumann, *The Physics of Inflation* (Lecture notes). University of Amsterdam.

[4] D. Fixsen, *The Temperature of the Cosmic Microwave Background*, The Astrophysical Journal, vol. 707, no. 2, pp. 916-920, 2009. Available: 10.1088/0004-637x/707/2/916.

[5] ESA and the Planck Collaboration. [online] Available at: `https://www.esa.int/ESA_Multimedia/Images/2013/03/Planck_CMB` [Accessed 6 July 2022].

[6] G. Watson, *A Treatise on the Theory of Bessel Functions* Pp. viii, 804. 70s. 1922. (Cambridge), The Mathematical Gazette, vol. 18, no. 231, pp. 349-350, 1934. Available: 10.2307/3605513.

[7] J. Silk, *Cosmic Black-Body Radiation and Galaxy Formation*, The Astrophysical Journal, vol. 151, p. 459, 1968. Available: 10.1086/149449.

[8] M. Kachelriess, *Quantum Fields*. [S.l.]: Oxford Univ Press US, 2022.

[9] Puicercus, A., 2022. *CMB-Power-Spectrum Repository*. [online] GitHub. Available at: `https://github.com/alfonsopuicer/CMB-Power-Spectrum` [Accessed 3 July 2022].

[10] R. Sachs and A. Wolfe, *Perturbations of a Cosmological Model and Angular Variations of the Microwave Background*, The Astrophysical Journal, vol. 147, p. 73, 1967. Available: 10.1086/148982.

[11] S. Dodelson, *Modern cosmology*. Academic Press, 2003.

[12] W. Hu and N. Sugiyama, *Anisotropies in the cosmic microwave background: an analytic approach*, The Astrophysical Journal, vol. 444, p. 489, 1995. Available: 10.1086/175624.

[13] W. Hu, *Lecture Notes on CMB Theory: From Nucleosynthesis to Recombination*. 2008, p. 41.

[14] W. Hu and S. Dodelson, *Cosmic Microwave Background Anisotropies*, Annual Review of Astronomy and Astrophysics, vol. 40, no. 1, pp. 171-216, 2002. Available: 10.1146/annurev.astro.40.060401.093926.

[15] W. Hu, *CMB Introduction*, background.uchicago.edu. [Online]. Available: `http://background.uchicago.edu/~whu/intermediate/score1a.html`. [Accessed: 25- June- 2022].